ARTICLE

Search for Past Life on Mars: Possible Relict Biogenic Activity in Martian Meteorite ALH84001

David S. McKay, Everett K. Gibson, Jr., Kathie L. Thomas-Keprta, Hojatollah Vali, Christopher S. Romanek, Simon J. Clemett, Xavier D. F. Chillier, Claude R. Maechling, and Richard N. Zare

Fresh fracture surfaces of the martian meteorite ALH84001 contain abundant polycyclic aromatic hydrocarbons (PAHs). These fresh fracture surfaces also display carbonate globules. Contamination studies suggest the PAHs are indigenous to the meteorite. High resolution scanning and transmission electron microscopy study of surface textures and internal structures of selected carbonate globules show that the globules contain fine-grained, secondary phases of single-domain magnetite and Fe-monosulfides. The carbonate globules are similar in texture and size to some terrestrial bacterially induced carbonate precipitates. Although inorganic formation is possible, formation of the globules by biogenic processes could explain many of the observed features including the PAHs. The PAHs, the carbonate globules, and their associated secondary mineral phases and textures could thus be fossil remains of a past martian biota.

A long-standing debate over the possibility of present-day life on Mars was addressed by the Viking lander experiments in 1976. Although the results were generally interpreted to be negative for life in the tested surface soils, the possibility of life at other locations on Mars could not be ruled out (*1*). The Viking lander's mass spectrometry experiments failed to confirm the existence of organics for the martian surface samples analyzed. Furthermore, the Viking results contained no information on possible fossils. Another source of information about possible ancient martian life is the Shergotty-Nakhla-Chassigny (SNC) class of meteorites, which appear to have come to the Earth by impact events on Mars (*2*, *3*). We have examined ALH84001 collected in Antarctica and recently recognized as a meteorite from Mars (*4*). Our objective was to look for signs of past (fossil) life within the pore space or secondary minerals of the martian meteorites. Our task is difficult because we only have a small piece of rock from Mars and we are searching for martian biomarkers on the basis of what we know about life on Earth. Therefore, if there is a martian biomarker, we may not be able to recognize it, unless it is similar to an earthly biomarker. Additionally, no information is available on the geologic context of the rock on Mars.

ALH84001 is an igneous orthopyroxenite consisting of coarse-grained orthopyroxene [$(Mg,Fe)SiO_3$] and minor maskelynite ($NaAlSi_3O_8$), olivine [$(Mg,Fe)SiO_4$], chromite ($FeCr_2O_4$), pyrite (FeS_2), and apatite [$Ca_5(PO_4)_3$] (*4*–*6*). Its crystallized 4.5 billion years ago (Ga) (*6*). It records at least two shock events separated by a period of annealing. The age of the first shock event has been estimated to be 4.0 Ga (*7*). Unlike the other SNC meteorites, ALH84001 contains secondary carbonate minerals that form globules from 1 to ~250 μm across (*4*, *6*, *8*, *9*). These carbonate globules have been estimated to have formed 3.6 Ga (*10*). Petrographic and electron microprobe results (*4*, *11*) indicate that the carbonates formed at relatively high temperatures (~700°C), however, the stable oxygen isotope data indicate that the carbonates formed between 0° and 80°C (*12*). The carbonate globules are found along fractures and in pore spaces. Some of the carbonate globules were shock-faulted (*4*, *5*). This shock event occurred on Mars or in space, and thus rules out a terrestrial origin for the globules (*3*, *8*, *13*). The isotopic composition of the carbon and oxygen associated with the carbonate globules also indicates that they are indigenous to the meteorite and were not formed during its 13,000-year residence in the Antarctic environment (*13*).

The $\delta^{13}C$ values of the carbonate in ALH84001 range up to 42 per mil for the large carbonate spheroids (*12*) and are higher than values for carbonates in other SNC meteorites. The source of the carbon is the martian atmospheric CO_2, which has been recycled through water into the carbonate (*12*). The carbon isotopic compositions of ALH84001 are similar to those measured in CM2 carbonaceous chondrites (*14*). Consequently, the carbonates in ALH84001 and the CM2 meteorites are believed to have been formed by aqueous processes on parent bodies. The $\delta^{13}C$ in martian meteorite carbonates ranges from −17 to +42‰ (*12*, *15*, *16*). This range of ^{13}C valves exceeds the range of ^{13}C generated by most terrestrial inorganic processes (*17*, *18*). Alternatively, biogenic processes are known to produce wide ranges in ^{13}C fractionations on Earth (*19*, *20*).

ALH84001 arrived on Earth 13,000 years ago and appears to be essentially free of terrestrial weathering (*8*). ALH84001 does not have the carbon isotopic compositions typically associated with weathered meteorites (*12*, *15*) and detailed mineralogical studies (*8*) show that ALH84001 has not been significantly affected by terrestrial weathering processes.

ALH84001 is somewhat friable and breaks relatively easily along preexisting fractures. It is these fracture surfaces that display the carbonate globules. We analyzed freshly broken fracture surfaces on small chips of ALH84001 for polycyclic aromatic hydrocarbons (PAHs) using a microprobe two-step laser mass spectrometer (μL²MS) (*22*, *23*).

Polycyclic aromatic hydrocarbons. Spatial distribution maps of individual PAHs on interior fracture surfaces of ALH84001 demonstrate that both total PAH abundance and the relative intensities of individual species have a heterogeneous distribution at the 50-μm scale. This distribution appears to be consistent with partial geochromatographic mobilization of the PAHs (*24*). The average PAH concentration in the interior fracture surfaces is estimated to be in excess of 1 part per million (*25*). The PAHs were found in highest concentration in regions rich in carbonates.

From averaged spectra we identified two groupings of PAHs by mass (Fig. 1A). A middle-mass envelope of 178 to 276 atomic mass units (amu), dominates and is composed mostly of simple 3- to 6-ring PAH skeletons with alkylated homologs accounting for less than 10% of the total integrated signal intensity. Principal peaks at 178, 202, 228, 252, and 278 amu are assigned to

D. S. McKay Mail Code SN, NASA Lyndon B. Johnson Space Center, Houston, TX 77058, USA.
E. K. Gibson, Jr., Mail Code SN4, NASA Lyndon B. Johnson Space Center, Houston, TX 77058, USA.
K. L. Thomas-Keprta, Lockheed Martin, Mail Code C23, 2400 NASA Road 1, Houston, TX 77058, USA.
H. Vali, Dept. of Earth and Planetary Sciences, McGill University, 3450 University St., Montreal, Quebec, H3A 2A7 Canada.
C. S. Romanek, Savannah River Ecology Laboratory, Drawer E, University of Georgia, Aiken, SC 29802, USA.
S. J. Clemett, X. D. F. Chillier, C. R. Maechling, R. N. Zare, Department of Chemistry, Stanford University, Stanford, CA 94305-5080, USA.

phenanthrene ($C_{14}H_{10}$), pyrene ($C_{16}H_{10}$), chrysene ($C_{18}H_{12}$), perylene or benzopyrene ($C_{20}H_{12}$), and anthanthracene ($C_{22}H_{12}$) (26). A second weak, diffuse high-mass envelope extends from about 300 to beyond 450 amu. The peak density is high and shows a periodicity at 14 and 2 amu. This distribution implies that there is a complex mixture of PAHs whose parent skeletons have alkylated side chains with varying degrees of dehydrogenation; specific assignments are ambiguous.

Contamination checks and control experiments indicate that the observed organic material is indigenous to ALH84001. The accumulation of PAHs on the Greenland ice sheet over the past 400 years has been studied in ice cores (27). The total concentration of PAHs in the cores varies from 10 parts per trillion for preindustrial times to 1 part per billion for recent snow deposition. Because Antarctica is in the less industrialized Southern Hemisphere, we may expect concentrations of PAHs in Antarctic ice to lie between these two limits. The primary source of PAHs is anthropogenic emissions, which are characterized by extensive alkylation (~10 fold greater than that of the parent PAHs) (28) and by the presence of abundant aromatic heterocycles, primarily dibenzothiophene ($C_{12}H_8S$; 184 amu). In contrast, the PAHs in ALH84001 are present at the part per million level (~10^3 to 10^5 times higher concentration), show little alkylation, and dibenzothiophene was not observed in any of the samples we studied.

Analysis of Antarctic salt deposits on a heavily weathered meteorite (LEW 85320) by μL^2MS did not show the presence of terrestrial PAHs within detection limits, which suggests an upper limit for terrestrial contamination of ALH84001 of 1%. Measurements of four interior fragments of two Antarctic ordinary chondrites (ALH83013 and ALH83101) of petrologic classes H6 and L6 showed no evidence of indigenous PAHs. These represent equivalent desorption matrix blanks; previous studies have shown that no indigenous organic material is present in meteorites of petrologic class six (29).

Spatially resolved studies of exterior fragments of ALH84001, with intact fusion crust show that no PAHs are present within the fusion crust or a zone extending into the interior of the meteorite to a depth of ~500 μm (Fig. 1, B–E). The PAH signal increases with increasing depth, leveling off at ~1200 μm within the interior, well away from the fusion crust. This concentration profile is consistent with volatilization and pyrolysis of indigenous PAHs during atmospheric entry of the meteorite and formation of a fusion crust (30) but inconsistent with terrestrial introduction of organic material into the interior of ALH84001 along cracks and pore spaces during burial in the Antarctic ice sheet. These results indicate that the PAHs are indigenous to ALH84001.

No evidence can be found for laboratory-based contamination introduced during processing. Samples for analysis were prepared at the meteorite clean labs at NASA Johnson Space Center and sealed in containers before they were transported to Stanford University. A contamination study conducted prior to analysis of these samples showed no evidence for any PAH contamination (31). We also conducted experiments in which chips of ALH84001 were cultured in nutrient medium under aerobic and anerobic conditions; we found the chips to be sterile.

PAHs have been found in a wide range of extraterrestrial materials using the μL^2MS technique, including carbonaceous and ordinary chondrites (29), interplanetary dust particles (2[illegible]32) and interstellar graphite grains (33). Each material is characterized by differing PAH distributions reflecting the different environments in which the PAHs formed and their subsequent evolution (for example, as a result of aqueous alteration and thermal metamorphism). Comparison of the mass distribution of PAHs observed in ALH84001 with that of PAHs in other extraterrestrial materials indicates that the closest match is with the CM2 carbonaceous chondrites (34). The PAHs in ALH84001, however, differ in several respects from the CM2 chondrites: low-mass PAHs such as naphthalene ($C_{10}H_8$; 128 amu) and acenaphthalene ($C_{12}H_8$; 152 amu) are absent in ALH84001, the middle-mass envelope shows no alkylation, and the relative intensity of the 5- and 6-ring PAHs and the relative intensity and complexity of the extended high-mass distribution are different.

On Earth, PAHs are abundant as fossil molecules in ancient sedimentary rocks, coal, and petroleum where they are derived from chemical aromatization of biological precursors such as marine plankton and early plant life (35). In such samples, PAHs are typically present as thousands, if not hundreds of thousands, of homologous and isomeric series; in contrast, the PAHs we observed in ALH84001 appear to be relatively

4colorfig001

4colorfig001

Fig. 1. (A) Averaged mass spectrum of an interior, carbonate-rich, fracture surface of ALH84001. The spectrum represents the average of 1280 individual spectra defining an analyzed surface region of 750 by 750 μm mapped at a spatial resolution of 50 by 50 μm. (B-E) PAH signal intensity as a function of distance from the ALH84001 fusion crust for the four primary PAHs shown in (A). The fusion crust fragment, which showed no preexisting fractures, was cleaved immediately prior to analysis using a stainless steel scalpel and introduced in <2 minutes into the μL^2MS. Each plot represents a section perpendicular to the fusion crust surface which starts at the exterior and extends a distance of 1200 μm inward. The spatial resolution is 100 μm along the section line and is the average of a 2 by 2 array of 50 by 50 μm analyses, with each analysis spot being the summed average of 5 time-of-flight spectra.

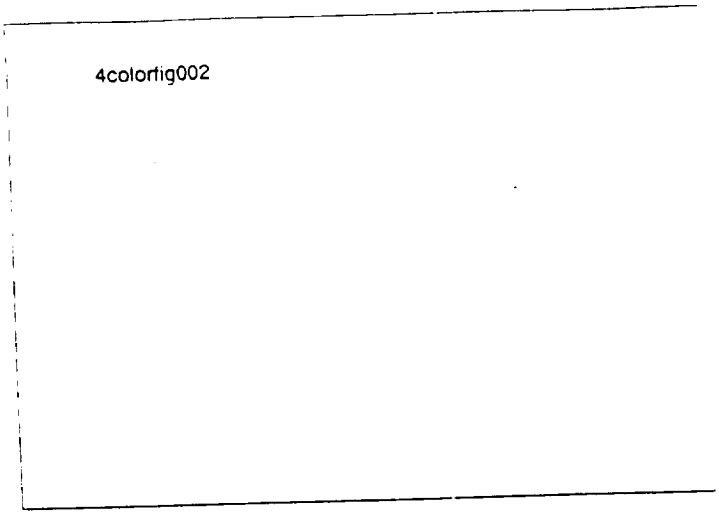

Fig. 2. False-color backscatter electron (BSE) image of fractured surface of a chip from ALH84001 meteorite showing distribution of the carbonate globules. Orthopyroxene is green and the carbonate globules are orange. Surrounding the Mg-carbonate are a black rim (magnesite) and a white, Fe-rich rim. Scale bar is 1 mm. (False color produced by C. Schwandt).

simple. The in situ chemical aromatization of naturally occurring biological cyclic compounds in early diagenesis can produce a restricted number of PAHs (36). Hence, we would expect that diagenesis of microorganisms on ALH84001 could produce what we observed—a few specific PAHs—rather than a complex mixture involving alkylated homologs.

Chemistry and mineralogy of the carbonates. The freshly broken, but preexisting fracture surfaces rich in PAHs also typically display carbonate globules. The globules tend to be discoid rather than spherical, and are flattened parallel to the fracture surface. Intact carbonate globules appear orange in visible light, have a rounded appearance, and many display alternating black and white rims. Under high magnification stereo light microscopy or SEM stereo imaging, some of the globules appear to be quite thin and pancake-like, suggesting that the carbonates formed in the restricted width of a thin fracture. This geometry limited their growth perpendicular to but not parallel to the fracture.

We selected a typical globule, ~50 μm in diameter, for analysis by TEM and electron microprobe (37). On the basis of backscatter electron (BSE) images (Fig. 2), the larger globules (>10 μm) have Ca-rich cores (which also contain the highest Mg abundances) surrounded by alternating Fe- and Mg-rich bands (Fig. 3). Near the edge of the globule, several sharp thin bands are present. The first band is rich in Fe and S, the second is rich in Mg with no Fe, the third is rich in Fe and S again (Fig. 3). Detectable S is also present in patchy areas throughout the globule.

In situ TEM analyses of the globule in Fig. 4 revealed that Fe- and Mg-rich carbonates located nearer to the rim range in composition from ferroan magnesite to pure magnesite. The Fe-rich rims are composed mainly of fine-grained magnetite ranging in size from ~10 to 100 nm and minor amounts of pyrrhotite (~5 vol%) (Figs. 3, region i and 4A). Magnetite crystals are cuboid, teardrop, and irregular in shape. Individual crystals have well-preserved structures with no lattice defects. The magnetite and Fe-sulfide are in a fine-grained carbonate matrix (Figs. 4A–4C). Composition of the fine-grained carbonate matrix matches that of coarse-grained carbonates located adjacent to the rim (Fig. 4A).

High-resolution transmission electron microscopy (HRTEM) and energy dispersive spectroscopy (EDS) showed that the Fe sulfide phase associated with the Fe-rich rims is pyrrhotite (Fig. 4C). Pyrrhotite particles are composed of S and Fe only, no oxygen was observed in the spectra; particles have atomic Fe/S ratios ranging from ~0.92 to 0.97. The size and shape of the FeS particles varies. Single euhedral crystals of pyrrhotite range up to ~100 nm across; polycrystalline particles have more rounded shapes ranging from ~20 to 60 nm across (Fig. 4C). HRTEM of these particles showed that their basal spacing is 0.57 nm, which corresponds to the {111} reflection of the pyrrhotite in a 4C monoclinic system. The magnetite is distributed uniformly in the rim, whereas the pyrrhotite seems to be distributed randomly in distinct domains ~5 to 10 μm long (Fig. 3C). Magnetite grains in ALH84001 did not contain detectable amounts of minor elements. In addition, these magnetite grains are single-domain crystals having no structural defects.

A distinct region, located toward the core of the carbonate spheroid but completely separate from the magnetite-rich rim described above, also shows accumulations of magnetite and an Fe-rich sulfide (Fig. 5A, region II and 5A). This region contains two types of textures: The first one is fine-grained massive and electron-dense under [illegible]. The second region is much less electron-dense and is porous. The porous texture occurs mainly in crosscutting fractures and rarely in isolated patches. We interpret this porous texture as a region

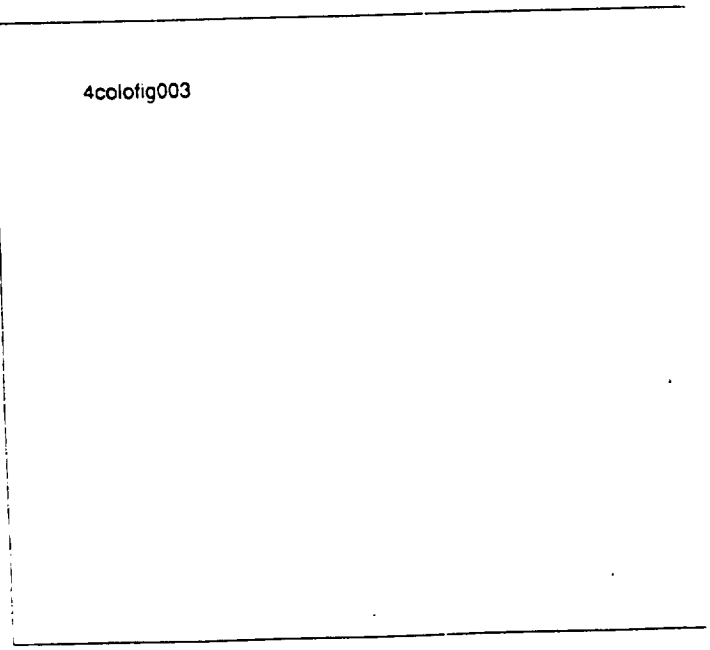

Fig. 3. BSE image and electron microprobe maps showing the concentration of five elements in a carbonate from ALH84001. The element maps show that the carbonate is chemically zoned. Colors range through red, green, light blue, and deep blue, reflecting the highest to lowest element concentrations. Scale bars for all images are 20 μm. (A) BSE image showing location of orthopyroxene (OPX), clinopyroxene (CPX), apatite (A), and carbonate (MgC, C). Fe-rich rims (R) separate the center of the carbonate (C) from a Mg-rich carbonate (MgC) rim. Region in the box is described in Figs. 5 and 6. (B) Fe is most abundant in the parallel rims, ~3 μm across, and in a region of the carbonate ~20 μm in size. (C) Highest S is associated with an Fe-rich rim; it is not homogeneously distributed, but rather located in discrete 3 regions or hot spots in the rim. A lower S abundance is present throughout the globule in patchy areas. (D) Higher concentrations of Mg are shown in the Fe-poor outer region of the carbonate. A Mg-rich region (MgC), ~8 μm across, is located between the two Fe-rich rims. (E) Ca-rich regions are associated with the apatite, the Fe-rich core of the carbonate and the clinopyroxene (F). P-rich regions are associated with the apatite.

which the massive carbonate has been partially dissolved. The nanometer-size magnetite and Fe-sulfide phases are everywhere associated with the fine-grained Mg-Fe-rich carbonate. In the regions containing high concentrations of magnetite, dissolution of carbonate is evident (Fig. 5A). In contrast to the magnetite-rich rim, the core area contains few magnetite particles. The Fe-sulfide phases in this magnetite-poor region have chemical compositions similar to that of the pyrrhotite. However, unlike pyrrhotite grains that have a large variety of morphologies, most of these Fe-sulfide particles have elongated shapes (Fig. 5B). We could not obtain a diffraction pattern of these Fe-monosulfide particles because they were unstable in the electron beam. Possible candidates for these Fe-monosulfide minerals include mackinawite (FeS_{1-x}), greigite (Fe_3S_4), and smythite (Fe_9S_{11}). Because of the morphological similarity to terrestrial greigite (Fig. 5C), we suggest these Fe sulfide minerals are probably greigite (38).

Formation of the magnetite and iron sulfides. The occurrence of the fine-grained carbonate, Fe-monosulfide, and magnetite phases could be explained by either inorganic or biogenic processes. Single-domain magnetite can precipitate inorganically under ambient temperature and neutral pH conditions by partial oxidation of ferrous solutions (39). This synthetic magnetite ranges in size from about 1 to more than 100 nm and is chemically very pure (39). Simultaneous inorganic precipitation of magnetite and pyrrhotite requires strongly reducing conditions at high pH (40). However, carbonate is normally stable at high pH, and the observed dissolution of carbonate would normally require low pH acidic conditions. It is possible that the Fe-sulfides, magnetite, and carbonates all formed under high pH conditions, and the acidity changed at some point to low pH causing the partial dissolution of the carbonates. But the Fe-sulfide and magnetite do not appear to have undergone any corrosion or dissolution (41), which would have likely occurred under acidic conditions. Moreover, as previously mentioned, the dissolution of carbonate is always intimately associated with the presence of Fe-sulfides and magnetite. Consequently, neither simultaneous precipitation of Fe-sulfides and magnetite along with dissolution of carbonates nor sequential dissolution of carbonate at a later time without concurrent dissolution of Fe-sulfides and magnetite seems plausible in simple inorganic models, although more complex models could be proposed.

In contrast, the coexistence of magnetite and Fe-sulfide phases within partially dissolved carbonate could be explained by biogenic processes, which are known to operate under extreme disequilibrium conditions. Intercellular coprecipitation of Fe-sulfides and magnetite within individual bacteria has been reported (42). In addition, extracellular biomediated precipitation of Fe-sulfides and magnetite can take place under anaerobic conditions (43, 44).

Magnetite particles in ALH84001 are similar (chemically, structurally, and morphologically) to terrestrial magnetite particles known as magnetofossils (45), which are fossil remains of bacterial magnetosomes (46) found in a variety of sediments and soils (41, 47, 48) and classified as single-domain (~20 to 100 nm) or superparamagnetic (<20 nm) (49). Single-domain magnetite has been reported in ancient limestones and interpreted as biogenic (48). Some of the magnetite crystals in the ALH84001 carbonates resemble extracellular precipitated superparamagnetic magnetite particles produced by the growth of anaerobic bacterium strain GS-15 (43).

Surface features and origin of the carbonates. We examined carbonate surfaces on a number of small chips of ALH84001 using high-resolution SEM (50). The Fe-rich rim of globules typically consist of an aggregate of tiny ovoids intermixed with small irregular to angular objects (Fig. 6A). Ovoids in the example are about 100 nm in longest dimension, and the irregular objects range from 20 to 80 nm across. These features are typical of those on the Fe-rich rims of many carbonate globules. These objects are similar in size and shape to features in the Fe-rich rims identified as magnetite and pyrrhotite (Figs. 4B-4C). These objects are too small to obtain compositional analysis under the SEM.

In the center of some of the globules (Fig. 2), the surface of the carbonate shows an irregular, grainy texture. This surface texture does not resemble either cleavage or a growth surface of synthetic and diagenetic carbonates (51). These surfaces also display small regularly shaped ovoid and elongated forms ranging from about 20 to 100 nm in longest dimension (Fig. 6B). Similar textures containing ovoids have been found on the surface of calcite concretions grown from Pleistocene ground water in southern Italy (52) where they are interpreted as nannobacteria that have assisted the calcite precipitation.

The origin of these textures on the surface of the ALH84001 carbonates (Fig. 6A–6B) is unclear. One possible explanation is that the textures observed on the carbonate surface is a result of the partial dissolution of the carbonate, that is they are erosional remnants of the carbonate that happen to be in the shape of ovoids and elongate forms perhaps because the carb-

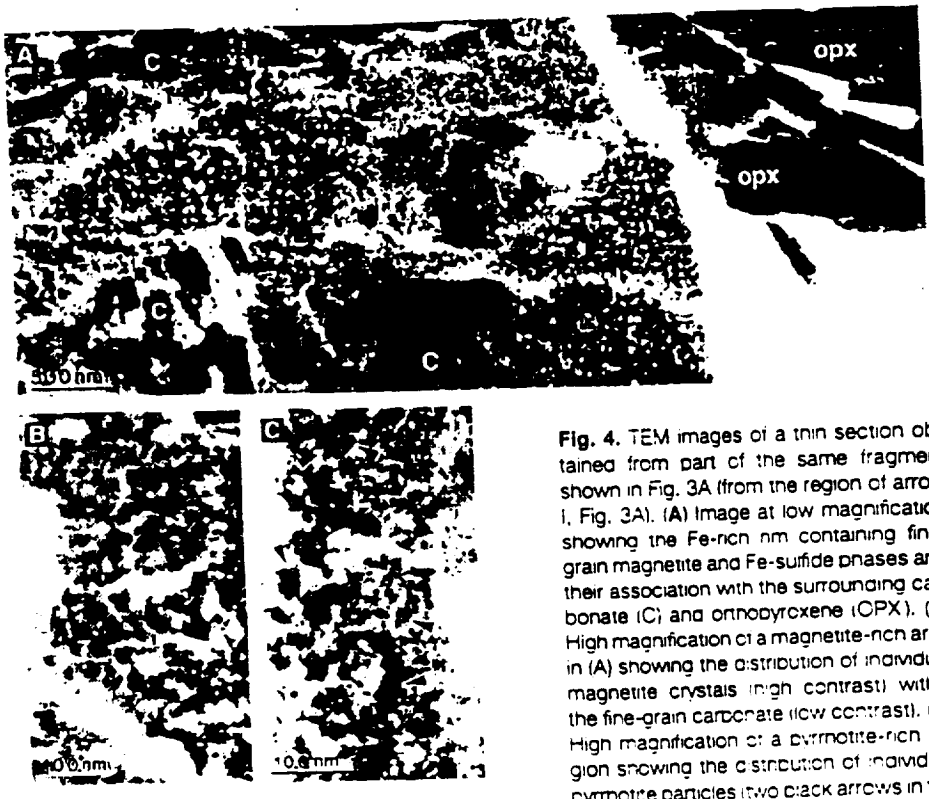

Fig. 4. TEM images of a thin section obtained from part of the same fragment shown in Fig. 3A (from the region of arrow 1, Fig. 3A). **(A)** Image at low magnification showing the Fe-rich rim containing fine-grain magnetite and Fe-sulfide phases and their association with the surrounding carbonate (C) and orthopyroxene (OPX). **(B)** High magnification of a magnetite-rich area in (A) showing the distribution of individual magnetite crystals (high contrast) within the fine-grain carbonate (low contrast). **(C)** High magnification of a pyrrhotite-rich region showing the distribution of individual pyrrhotite particles (two black arrows in the center) together with magnetite (other arrows) within the fine-grained carbonate (low contrast).

Orig. Cc. OPERATOR: | Session | PROOF: | PE's: | AA's: | COMMENTS: ARTNO:
1st Disk, 2nd | sheila | 6

ate has preferentially eroded along grain boundaries or dislocations. Shock effects may have enhanced such textures. However, as we know of no similar example from the terrestrial geologic record or from laboratory experiments, we cannot fully evaluate this possible explanation for the textures. A second possibility is that artifacts can be created during sample preparation or may result from laboratory contamination. For example, the application of a thick Au-conductive coating can produce textures resembling mud cracks, and even droplets or blobs of Au. Laboratory contamination can include dust grains, residue from sample cleaning, and organic contamination from epoxy. For comparison, we examined several control samples treated identically to the meteorite chips. We conclude that the complex textures (Fig. 6) did not result from procedures used in our laboratory. Only interior or freshly broken surfaces of chips were used (52). We did observe an artifact texture from our Au-Pd conductive coating that consists of a mud crack-like texture visible only at 50,000× magnification or greater. None of the controls display concentrations or blobs of coating material. A lunar rock chip carried through the same procedures and examined at high magnification showed none of the features seen in Fig. 6.

An alternative explanation is that these textures as well as the nanosize magnetite and Fe-sulfides, are the products of microbiological activity. It could be argued that these features in ALH84001 formed in Antarctica by biogenic processes or inorganic weathering. It is unlikely that reduced phases, such as iron sulfides, would form in Antarctica during inorganic weathering; reported authigenic sulfur-bearing phases from Antarctic soils and meteorites are sulfates or hydrated sulfates. In general, authigenic secondary minerals in Antarctica are oxidized or hydrated (53). The lack of PAHs in the analyzed Antarctic meteorites, the sterility of the sample, and the nearly unweathered nature of ALH84001 argue against an Antarctic biogenic origin. As a control we examined three Antarctic ordinary chondrites (ALH78119, ALH76004, and ALH81021) (which do not have indigenous PAHs) from the same ice field where ALH84001 was collected, as well as a heavily weathered ordinary chondrite that gave negative results for PAHs (LEW 85320). These meteorites were chosen to cover the different degrees of weathering observed on Antarctic meteorites. Examination of grain surfaces at all magnifications in weathered and unweathered regions of these meteorites showed no sign of the ovoid and elongate forms seen in ALH84001. However, none of these control meteorites contained detectable carbonate.

Ovoid features in Fig. 6 are similar in size and shape to nannobacteria in travertine and limestone (54). The elongate forms (Fig. 6B) resemble some forms of fossilized filamentous bacteria in the terrestrial fossil record. In general, the terrestrial bacterial microfossils (55) are more than an order of magnitude larger than the forms seen in the ALH84001 carbonates.

The carbonate globules in ALH84001 are clearly a key element in the interpretation of this martian meteorite. The origin of these globules is controversial; Harvey and McSween (11) and Mittlefehldt (4) argue on the basis of microprobe chemistry and equilibrium phase relationships, that the globules were formed by high-temperature metamorphic or hydrothermal reactions. Alternatively, Romanek *et al.* (12) argue on the basis of isotopic relationships that the carbonates were formed under low-temperature hydrothermal conditions (50°C). The nanophase magnetite and iron monosulfides present in these globules would probably not be detected in microprobe analyses, which normally have a spatial resolution of about 1 micrometer. Our TEM observations and our S maps suggest that nanophase magnetite and iron sulfides, while present in some zones, are present throughout the globules. The effect of these fine-grained oxide and sulfide minerals on bulk microprobe analyses must be considered in the interpretation of the microprobe

Fig. 5. TEM images of a thin section showing the morphology of the Fe-sulfide phases present in ALH84001 and a terrestrial soil sample. Iron sulfide phase (greigite?—Fe_3S_4) is located in a magnetite-poor region separate and distinct from the magnetite-rich rims (Fig. 3A, arrow II). (**A**) TEM of a thin section showing a cross section of a single carbonate crystal (large black regions: The apparent cleavage features are due to knife damage by ultramicrotomy.) A vein of fine-grained carbonate (light grey) is observed between the large carbonate crystal. Possibly greigite and secondary magnetite (fine, dark crystals) have been precipitated in this fine-grained matrix. There is a direct relation between the degree of carbonate dissolution and the concentration of the fine-grained magnetite and Fe-sulfide phases. This region shows less alteration of carbonate and fewer Fe-rich particles, while regions shown in Fig. 4 contain carbonate that has been highly altered and contains abundant Fe-rich particles. The cleavage surface of the carbonate crystal does not show any dissolution features (arrows); there is no evidence of structural selective dissolution of carbonate. (**B**) a representative elongated Fe-sulfide particle, located in the dissolution region of the carbonate described in (A), is most likely composed of greigite. The morphology and chemical composition of these particles are similar to the biogenic greigite described in (C). (**C**) High magnification of an individual microorganism within a root cell of a soil sample showing an elongated, multicrystalline core of greigite within an organic envelope.

Fig. 6. High-resolution SEM images showing ovoid and elongate features associated with ALH84001 carbonate globules. (**A**) Surface of Fe-rich rim area. Numerous ovoids, approximately 100 nm in diameter, are present (arrows). Tubular-shaped bodies are also apparent (arrows). Smaller angular grains may be the magnetite and pyrrhotite found by TEM. (**B**) Close view of central region of carbonate (away from rim areas) showing textured surface and nanometer ovoids and elongated forms (arrows).

(4, 11) uncertain. Alternatively, if the globules are products of biologic activity, a low-temperature formation would be indicated. The textures of the carbonate globules are similar to bacterially induced carbonate crystal bundle precipitates produced in the laboratory and in a fresh water pond (57). Moreover, the observed sequence in the martian carbonate globules—Mn-containing carbonate production early (in the core) followed by Fe carbonate and finishing with the abundant production of reduced Fe-sulfides is a sequence that is common in terrestrial settings, as Mn is first reduced by biogenic action, followed by ferric iron and sulfate (57). Pure Mg-carbonate (magnesite) can also be produced by biomineralization under alkaline conditions (59). On the basis of these observations, we interpret that the carbonate globules have a biogenic origin and were likely formed at low temperatures.

It is possible that all of the described features in ALH84001 can be explained by inorganic processes, but these explanations appear to require restricted conditions, for example sulfate reducing conditions in Antarctic ice sheets, which are not known to occur. Formation of the described features by organic activity in Antarctica is also possible but such activity is only poorly understood at present. However, many of the described features are closely associated with the carbonate globules which, based on textural and isotopic evidence, were likely formed on Mars before the meteorite came to Antarctica. Consequently, the formation of possible organic products (magnetite and iron-monosulfides) within the globules is difficult to understand, if the carbonates formed on Mars and the magnetite and iron monosulfides formed in Antarctica. Additionally, these products might require anerobic bacteria, and the Antarctic ice sheet environment appears to be oxygen-rich; ferric oxide formed from metallic Fe is a common weathering product in Antarctic meteorites.

In examining the martian meteorite ALH84001 we have found that the following evidence is compatible with the existence of past life on Mars: (i) an igneous Mars rock (of unknown geologic context) that was penetrated by a fluid along fractures and pore spaces, which then became the sites of secondary mineral formation and possible biogenic activity, (ii) a formation age for the carbonate globules younger than the age of the igneous rock, (iii) SEM and TEM images of carbonate globules and features resembling terrestrial microorganisms, terrestrial biogenic carbonate structures, or microfossils, (iv) magnetite and iron sulfide particles that could have resulted from oxidation and reduction reactions known to be important in terrestrial microbial systems, (v) the presence of PAHs associated with surfaces rich in carbonate globules. None of these observations is in itself conclusive for the existence of past life. Although there are alternative explanations for each of these phenomena taken individually, when considered collectively, particularly in view of their spatial association, we conclude that they are evidence for primitive life on early Mars.

REFERENCES AND NOTES

1. P. Mazur *et al.*, *Space Sci. Rev.* **22**, 3 (1978); H. P. Klein, *Eos* **76**, 334 (1995).
2. H. J. Melosh, *Icarus* **59**, 234 (1984); B. J. Gladman, J. A. Burns, M. Duncan, P. Lee, H. F. Levison, *Science* **271**, 1387 (1996).
3. H. P. McSween Jr., *Meteoritics* **29**, 757 (1994). Analyses of the gases in glassy inclusions in the SNC meteorites EET79001 by Bogard and Johnson [*Science* **221**, 651 (1983)], Becker and Pepin [*Earth Planet. Sci. Lett.* **69**, 225 (1983)], and Marti *et al.* [*Science* **267**, 1981 (1995)] have shown that the abundance and isotopic compositions of the trapped gases in the SNC meteorites and the measured atmospheric compositions on Mars, measured in situ by the Viking landers, have a direct one-to-one correlation (over nine orders of magnitude in concentrations). This remarkable agreement is one of the strongest arguments that the SNC meteorites represent samples from Mars.
4. D. W. Mittlefehldt, *Meteoritics* **29**, 214 (1994).
5. A. H. Treiman, *ibid.* **30**, 294 (1995).
6. E. Jagoutz, A. Sorowka, J. D. Vogel, H. Wänke, *ibid.* **29**, 478 (1994); L. E. Nyquist, B. M. Bansal, H. Wiesmann, C. Y. Shih, *Lunar Planet. Sci.* **26**, 1065 (1995).
7. R. D. Ash, S. F. Knott, G. Turner, *Nature* **380**, 57 (1996).
8. S. J. Wentworth and J. L. Gooding, *Lunar Planet. Sci.* **26**, 1489 (1995).
9. K. L. Thomas *et al.*, *ibid.*, p. 1409.
10. S. K. Knott, R. D. Ash, G. Turner, *ibid.*, p. 765.
11. R. Harvey and H. P. McSween Jr., *Nature* **382**, 49 (1996).
12. C. S. Romanek *et al.*, *ibid.* **372**, 655 (1994).
13. J. L. Gooding, *Icarus* **99**, 28 (1992).
14. M. M. Grady, I. P. Wright, P. K. Swart, C. T. Pillinger, *Geochim. Cosmochim. Acta* **52**, 2855 (1988).
15. A. J. T. Jull, C. J. Eastoe, S. Xue, G. F. Herzog, *Meteoritics* **30**, 311 (1995).
16. R. H. Carr, M. M. Grady, I. P. Wright, C. T. Pillinger, *Nature* **314**, 248 (1985); I. P. Wright, C. P. Hartmetz, C. T. Pillinger, *J. Geophys. Res.* **98**, 3477 (1993).
17. A. J. T. Jull, S. Cloudt, C. J. Eastoe, Workshop on Evolution of Martian Volatiles, *Lunar Planet. Inst. Tech. Rep. 96-01*, Part 1, 22 (Lunar and Planetary Institute, Houston, TX, 1996); J. D. Hudson, *J. Geol. Soc. London* **133**, 637 (1977).
18. I. D. Clark and B. Launol, *Chem. Geol.* **102**, 217 (1992); N. Nakai, H. Wada, Y. K. Iyosu, M. Takimoto, *Geochem. J.* **9**, 7 (1975).
19. K. J. Murata, I. Friedman, B. M. Madsen, *U.S. Geol. Surv. Prof. Pap. 614B*, 1 (1969); A. M. Martini, L. M. Walter, J. M. Budai, T. C. W. Ku, *Geol. Soc. Am. Abstr. Prog.* **27**, A292 (1995); G. E. Claypool and I. R. Kaplan, in *Natural Gases in Marine Sediments*, I. R. Kaplan, ed. (Plenum, NY, 1974), pp. 99–139.
20. T. O. Stevens and J. P. McKinley, *Science* **270**, 450 (1995).
21. When referring to the Martian meteorites, we use microorganism in a general sense—to signify a morphology that can be interpreted as fossilized microorganisms or small groupings of such organisms on the basis of our knowledge of terrestrial features.
22. μL^2MS was used to analyze fresh fractured samples of ALH84001 for the presence of PAHs. The μL^2MS instrument is capable of the simultaneous measurement of all PAHs present on a sample surface to a spatial resolution of 40 μm, and detection limits are in the sub-attomole ($>10^7$ molecules) range (1 attomol = 10^{-18} mol).
23. S. J. Clemett, C. R. Maechling, R. N. Zare, P. D. Swan, R. M. Walker, *Science* **262**, 721 (1993).
24. M. R. Wing and J. L. Bada, *Geochim. Cosmochim. Acta* **55**, 2937 (1991).
25. PAH concentration is estimated from comparison of the averaged spectra of interior fracture surfaces of ALH84001 with known terrestrial standards and the Murchison (CM2) meteorite matrix. In the case of Murchison (CM2), the total concentration of PAHs has been independently measured to be in the range of 18 to 28 parts per million [K. L. Pering and C. Ponnamperuma, *Science* **173**, 237 (1971)]. The average PAH spectrum of ALH84001 used in this estimate was generated from the average of ~4000 single-shot spectra acquired from three separate fracture surfaces encompassing an analyzed surface area of ~2 mm^2, representing regions both rich and poor in PAHs.
26. At a single laser ionization wavelength, μL^2MS is unable to distinguish between structural isomers; however, because different isomers have different photoionization cross sections, mass assignments are based on the most probable isomer. In the case of masses 178 and 202, the possible isomer combinations are phenanthrene or anthracene and pyrene or fluoranthene. At the photoionization wavelength used in this study, 266 nm, the μL^2MS instrument is ~19 times as sensitive to phenanthrene as to anthracene and ~23 times as sensitive to pyrene as to fluoranthene [R. Zenobi and R. N. Zare, in *Advances in Multiphoton Processes and Spectroscopy*, S. H. Lin, Ed. (World Scientific, Singapore, 1991), vol. 7, pp. 1–167]. Hence, masses 178 and 202 are assigned to phenanthrene and pyrene. In the case of higher masses, more structural isomers exist, and assignments are based on those PAHs known to have high cross sections from comparisons with standards.
27. K. Kawamura and I. Suzuki, *Naturwissenschaften* **81**, 502 (1994).
28. W. W. Youngblood and M. Blumer, *Geochim. Cosmochim. Acta* **39**, 1303 (1975); S. T. Wakeham, C. Schaffner, W. Giger, *ibid.* **44**, 403 (1980); R. E. LaFlamme and R. A. Hites, *ibid.* **42**, 289 (1978); T. E. Jensen and R. A. Hites, *Anal. Chem.* **55**, 594 (1983).
29. S. J. Clemett, C. R. Maechling, R. N. Zare, P. M. C. D. Alexander, *Lunar Planet. Sci.* **23**, 233 (1992); L. A. Kovalenko *et al.*, *Anal. Chem.* **64**, 682 (1992).
30. The interiors of stony meteorites are not heated above 100° to 120°C during passage through the Earth's atmosphere. For example, in the CI carbonaceous chondrite Murchison, amino acids have been found by Kvenvolden *et al.* [*Nature* **228**, 923 (1970)]. If temperatures had been above 120°C, amino acids would have degraded.
31. Sources of laboratory contamination fall into three categories: sample handling, laboratory air, and virtual leaks (that is, sources of PAHs inside the μL^2MS vacuum chamber). Possible contamination during sample preparation was minimized by performing nearly all sample preparation at the NASA-JSC meteorite curation facility. In cases where subsequent sample handling was required at Stanford, manipulation was performed in less than 15 minutes using only stainless steel tools previously rinsed and ultrasonicated in methanol and acetone. Dust-free gloves were worn at all times and work was performed on a clean aluminum foil surface. To quantify airborne contamination from exposure to laboratory air, two clean quartz discs were exposed to ambient laboratory environments both at NASA-JSC and Stanford. Each disc received an exposure typical of that experienced subsequently by samples of ALH84001 during sample preparation. No PAHs were observed on either quartz disk at or above detection limits. Because contamination can depend on the physical characteristics of the individual sample (for example, a porous material will likely give a larger contamination signal than a nonporous one) additional contamination studies have been previously conducted at Stanford [see (28)]. Briefly, samples of the meteorite acid residues of Barwell (L6) and Bishunpur (LL3.1) were exposed to laboratory air for 1 and 4 days

respectively. Barwell (L6) is known to contain no indigenous PAHs and none were observed on the exposed sample. Bishunpur (L3.1), in contrast, contains a rich suite of PAHs, but no discernible differences in signal intensities were observed between exposed and unexposed samples. To test for contamination from virtual leaks, the μL²MS instrument was periodically checked using samples of Murchison (CM2) meteorite matrix whose PAH distribution has been previously well characterized. No variations in either signal intensity or distribution of PAHs were observed for μL²MS instrument exposure times in excess of 3 days. No sample of ALH84001 was in the instrument for longer than 6 hours. The μL²MS vacuum chamber is pumped by an oil-free system: two turbomolecular pumps, and a liquid-nitrogen-cooled cryopump.

32. K. L. Thomas *et al.*, *Geochim. Cosmochim. Acta* **59**, 2797 (1995).
33. S. J. Clemett, S. Messenger, X. D. F. Chillier, X. Gao, R. M. Walker, R. N. Zare, *Lunar. Planet. Sci.* **26**, 229 (1996).
34. S. J. Clemett, Thesis, Stanford University (1996).
35. B. P. Tissot and D. H. Welte, *Petroleum Formation and Occurrence* (Springer, New York, 1978).
36. R. E. LaFlamme and R. A. Hites, *Geochim. Cosmochim. Acta* **42**, 289 (1978); S. G. Wakeham, C. Schaffner, W. Giger, *ibid.* **44**, 415 (1980).
37. We removed the spheroid from a thin section with a micro-coring device, embedded it in epoxy, thin sectioned it using an ultramicrotome, and analyzed it using a TEOL 2000FX TEM [technique described in (31)]. We made approximately 50 thin sections from the globule, and the remaining carbonate globule was coated with evaporated carbon for conductivity (~10 nm) and mapped with wavelength dispersive spectroscopy for major and minor elements using a Cameca SX 100 microprobe (Fig. 3).
38. H. Stanek, J. W. E. Fassbinder, H. Vali, H. W. Geiß, W. Graf, *Eur. J. Soil Sci.* **45**, 97 (1994).
39. B. A. Maher, in *Iron Biominerals*, R. B. Frankel and R. P. Blakemore, Eds. (Plenum, New York, 1991), pp. 179 (1991); R. M. Taylor, B. A. Maher, P. G. Self, *Clay Minerals* **22**, 411 (1987).
40. H. G. Machel, in *Palaeomagnetic Applications in Hydrocarbon Exploration and Production*, P. Turner and A. Turner, Eds. (*Geol. Soc. Spec. Publ.* **98**, Geological Society, London, 1998), pp. ●●; R. M. Garrels and C. L. Christ, *Solutions, Minerals and Equilibria*, (Freeman, Cooper and Co., San Francisco, 1969).
41. H. Vali and J. L. Kirschvink, *Nature* **339**, 203 (1989); H. Vali, O. Forster, G. Amarantidis, N. Petersen, *Earth Planet. Sci. Lett.* **86**, 389 (1987).
42. A. H. Vali and J. L. Kirschvink, in *Iron Biominerals* (R. B. Frankel and R. B. Blakemore, Eds), Plenum, 1990, pp. 97–1●●; S. Mann, N. H. C. Sparks, R. B. Frankel, D. A. Bazylinski, H. W. Jannasch, *Nature* **343**, 258 (1990); M. Fanna, D. M. Esquivel, H. G. P. L. de Barros, *ibid.*, p. 256 (1990); D. A. Bazylinski, B. R. Heywood, S. Mann, R. B. Frankel, *ibid.* **366**, 218 (1993); A. Demitrac, in *Magnetite Biomineralization and Magnetoreception*, J. Kirschvink, D. S. Jones, B. J. McFadden, Eds. (Plenum, New York, 1985, pp. 625–●●●; R. B. Frankel and R. B. Blakemore, Eds. *Iron Biomineralization*, (Plenum Press, NY) (1991).
43. D. R. Lovely, J. F. Stolz, G. L. Nord, Jr., E. J. P. Phillips, *Nature* **330**, 252 (1987).
44. D. Fortin, S. Davis, G. Southam, T. J. Beveridge, *J. Indust. Microbiol.* **14**, 178 (1995).
45. J. L. Kirschvink and S. B. R. Chang, *Geology* **12**, 559 (1984).
46. R. P. Blakemore, *Annu. Rev. Microbiol.* **36**, 217 (1982).
47. N. Petersen, T. von Dobeneck, H. Vali, *Nature* **320**, 611 (1986); J. W. E. Fassbinder, H. Stanjek, H. Vali, *ibid.* **343**, 161 (1990).
48. S. R. Chang, J. F. S. Tolz, J. L. Kirschvink, S. M. Awramik, *Precambrian Res.* **42**, 305 (1989).
49. R. F. Butler and S. K. Banerjee, *J. Geophys. Res.* **80**, 4049 (1975).
50. We hand picked small chips in a clean bench from our curatorial allocation of ALH84001. Most chips were from a region near the central part of the meteorite and away from the fusion crust, although for comparison we also looked at chips containing some fusion crust. For high resolution work we used a Au-Pd coating estimated to be ~2 nm thick in most cases. On some samples we used a thin (<1 nm) coating, about 10 s with our sputter coater; these samples usually showed charging effects and could not be used for highest resolution imaging. We more typically used 20 to 30 s. For backscatter and chemical mapping we used a carbon coat of about 5 to 10 nm thick. We monitored the possible artifacts from the coating using other reference samples or by looking at fresh mineral surfaces on ALH84001. We could also estimate relative coating thicknesses by the size of the Au and Pd peaks in the energy dispersive x-ray spectrum. For our heaviest coating, a slight crazing texture from the coating is barely visible at a magnification of 100,000× on the cleanest fresh grain surfaces. The complex textures shown in most of the SEM photographs are not an artifact of the coating process, but are the real texture of the sample. We used a JEOL 35 CF and a Philips SEM with a field emission gun (FEG) at the Johnson Space Center. The Jeol and Philips SEMs are equipped respectively with a PGT and Link EDS system. We achieved about 2.0 nm resolution at 30KV. Some images was also taken at lower kV, ranging from 1 to 10 kV. In most cases, the chips were coated after handpicking with no further treatment. For comparison, several chips were ultrasonically cleaned for a few seconds in liquid Freon before coating to remove adhering dust. Several samples were examined uncoated at low KV. We carbon-coated and examined all of the surfaces analyzed for PAHs only after the PAHs analyses had been completed.
51. J. Paquette, H. Vali, E. W. Mountjoy, *Am. Mineral.*, in press; J. Paquette, H. Vali, A. Mucci, *Geochim. Cosmochim. Acta*, in press.
52. E. F. McBride, M. Dane Picard, R. L. Folk, *J. Sed. Res.* **A64**, 535 (1994); see fig. 9.
53. E. K. Gibson, S. J. Wentworth, D. S. McKay, *Proc. 13th Lunar Planet. Sci. Conf., Part 2, J. Geophys. Res.* **88**, Suppl. A912 (1983); M. A. Velbel, *Meteoritics* **23**, 151 (1988); I. B. Campbell and G. G. C. Claridge, *Antarctica: Soils, Weathering Processes and Environment, Developments in Soil Science* 16 (Elsevier, Amsterdam, 1987).
54. R. L. Folk, *J. Sed. Petrol.* **63**, 990 (1993).
55. J. W. Schopf and C. Klein, Eds., *The Proterozoic Biosphere* (Cambridge Univ. Press, New York, NY 1992).
56. Contrary to the interpretations presented by Harvey and McSween (11) concerning the equilibrium partitioning of stable carbon isotopes on Mars, $\delta^{13}C$ values for carbonate and atmospheric CO_2 are incompatible with a high-temperature origin. For the $CaCO_3$-CO_2 system, solid carbonate is only enriched in ^{13}C below approximately 200°C [T. Chacko, T. K. Mayeda, R. N. Clayton and J. R. Goldsmith, *Geochim. Cosmochimica Acta* **55**, 2867 (1991); C. S. Romanek, E. L. Grossman and J. W. Morse, *Geochim. Cosmochimica Acta* **56**, 419 (1992)]. Assuming the $\delta^{13}C$ of ambient CO_2 is 27 per mil (the delta value for trapped gases in the Martian meteorite EETA79001 [C. P. Harzmetz, I. P. Wright, C. T. Pillinger, in *Workshop on the Mars Surface and Atmosphere through Time*, R. M. Haberle *et al.*, Eds (*Tech. Rep. 92-02*, Lunar and Planetary Institute, Houston, 1992, pp. 67–68], a $\delta^{13}C$ of 42 per mil for carbonate in ALH84001 can only be explained by a precipitation temperature around 0°C. This temperature estimate is compatible with an independent range of precipitation temperatures (0° to 80°C) based on the $\delta^{18}O$ of the same carbonates (12). If carbon isotopes are distributed heterogeneously on Mars in isolated reservoirs (for example, the crust and atmosphere), precipitation temperature estimates based on stable isotopes are relatively unconstrained. This is probably not the case though as other researchers [(3); L. L. Watson, I. D. Hutcheon, S. Epstein and E. M. Stolper, *Science* **265**, 86 (1994); B. M. Jakosky, *Geophys. Res. Lett.* **20**, 1591 (1993)] have documented a link between crustal and atmospheric isotopic reservoirs on the planet.
57. C. Buczynsik and H. S. Chafetz, *J. Sed. Petrol.* **61**, 226 (1991) (see Figs. 1D, 3A, and 3B).
58. K. N. Nealson and ●. ●. Saffarini, *Annu. Rev. Microbiol.* **48**, 311 (1994); J. P. Hendry, *Sedimentology* **40**, 87 (1993).
59. J. B. Thompson and F. G. Ferris, *Geology* **18**, 995 (1990).
60. We thank L. P. Keller, V. Yang, C. Le, R. A. Socki, M. F. McKay, M. S. Gibson, and S. R. Kepria for assistance. We thank R. Score and M. Lindstrom for their help in sample selection and preparation. The guidance of J. W. Schopf at an early stage of this study is appreciated. We also thank G. Horuchi, L. Hulse and L. _. Darrow, D. Pierson and personnel from Bldg. 37. The work was supported in part by NASA Planetary Materials Program (DSM and RNZ) and the Exobiology Program (DSM). Additional support from NASA-JSC Center Director's Discretionary Program (EKG) is recognized. C.S.R. and H.V. acknowledge support from the National Research Council. XDFC acknowledges support from the Swiss National Science Foundation.

● April 1996; accepted 16 July 1996

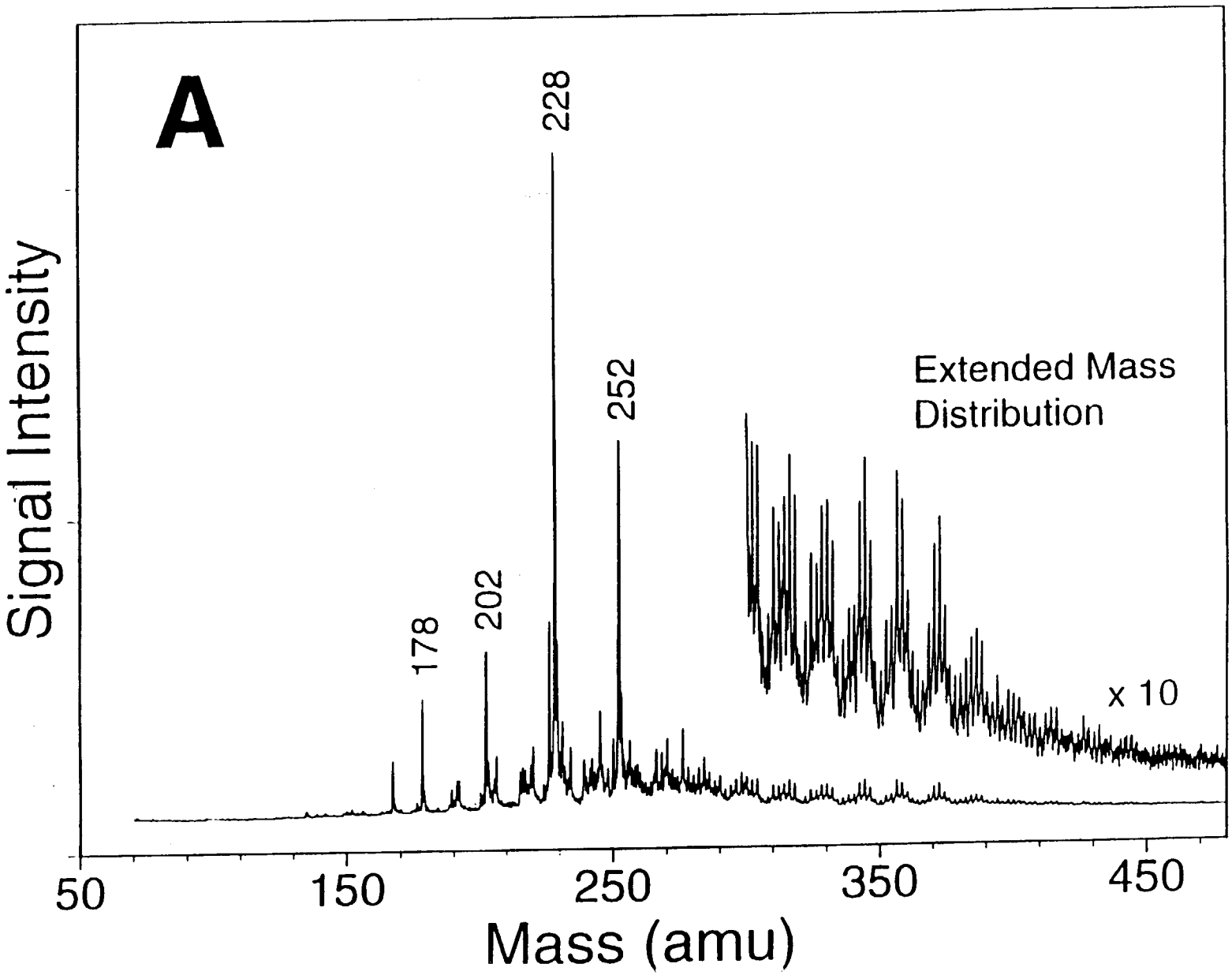
A
228
252
178
202
Extended Mass
Distribution
x 10
Signal Intensity
50
150
250
350
450
Mass (amu)

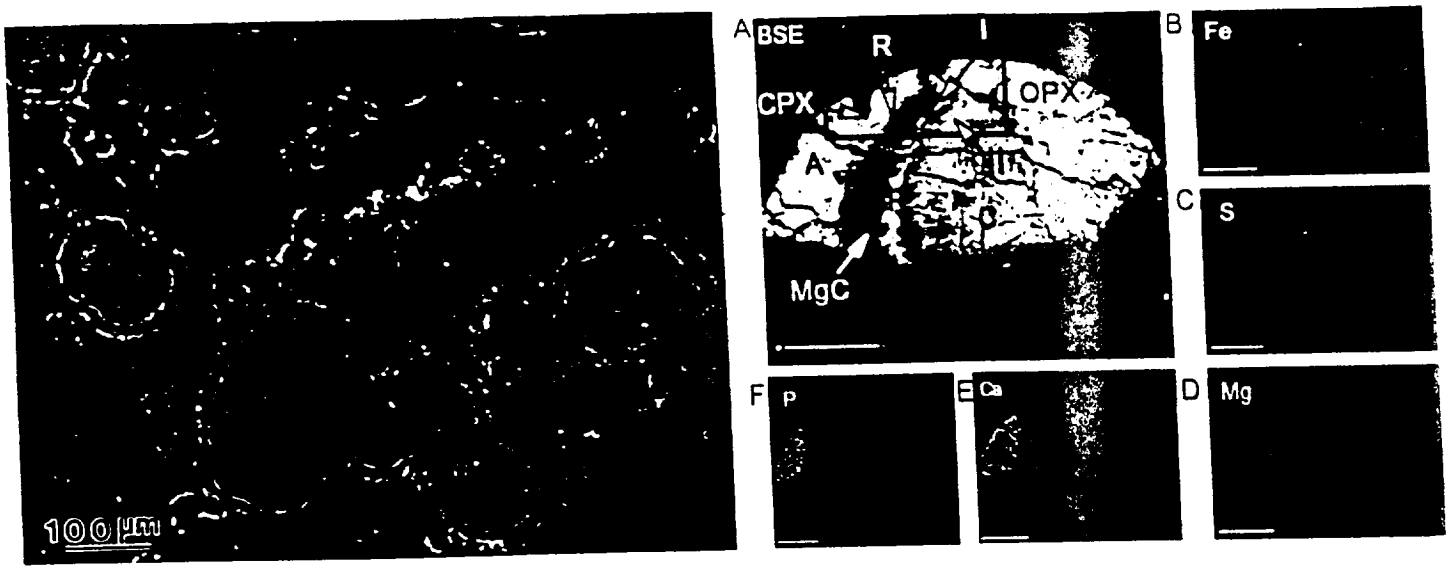
100 μm
A
BSE
R
I
CPX
OPX
A
MgC
B
Fe
C
S
D
Mg
E
Ca
F
P

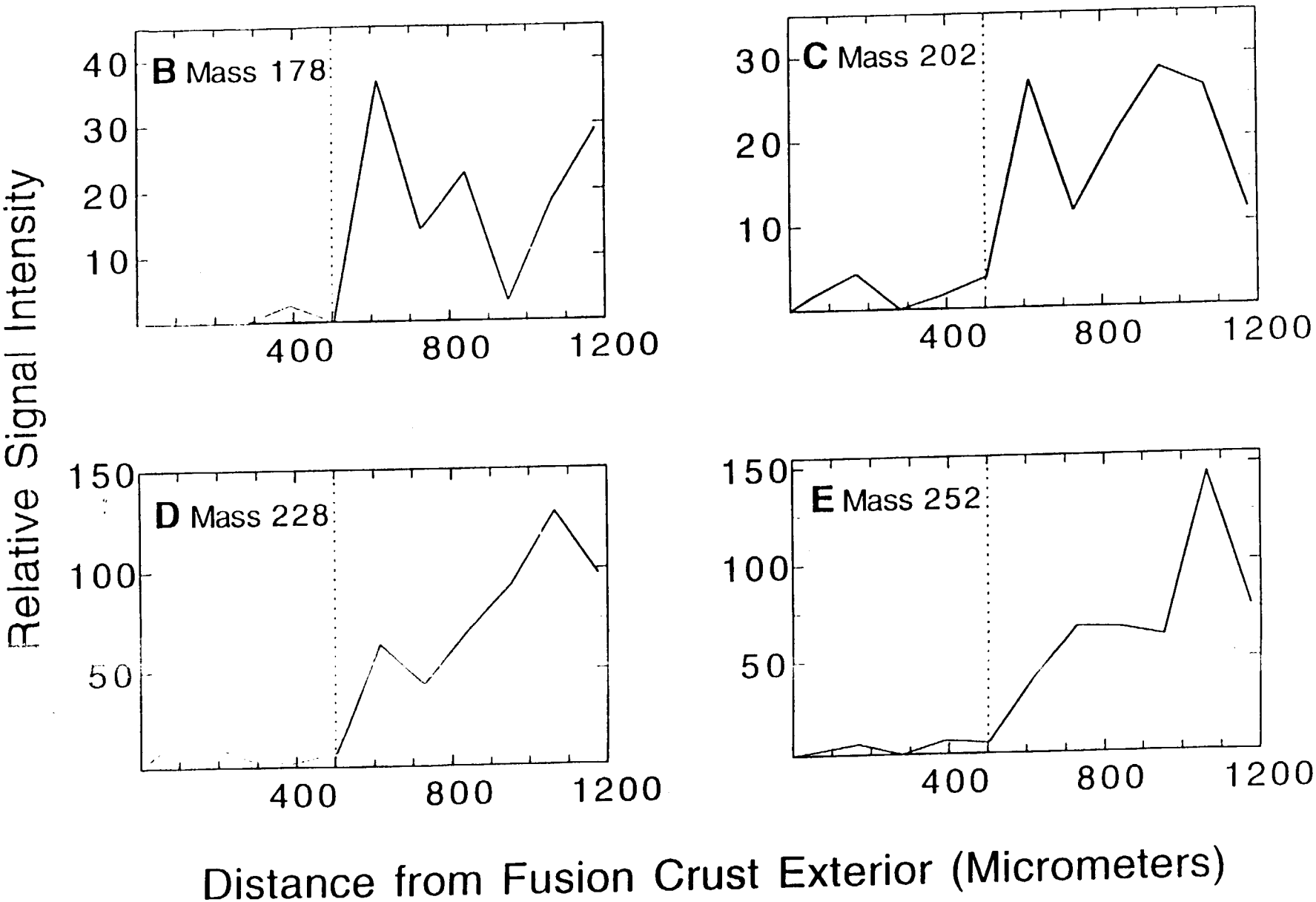
B Mass 178
C Mass 202
D Mass 228
E Mass 252
Relative Signal Intensity
Distance from Fusion Crust Exterior (Micrometers)
40
30
20
10
400
800
1200
150
100
50